Electric Model of the Vacuum Vessel of ZEPHYR

K.F. Mast

IPP 1/174 November 1979

MAX-PLANCK-INSTITUT FÜR PLASMAPHYSIK

8046 GARCHING BEI MÜNCHEN

MAX-PLANCK-INSTITUT FÜR PLASMAPHYSIK

GARCHING BEI MÜNCHEN

Electric Model of the Vacuum Vessel of ZEPHYR

K.F. Mast

IPP 1/174 November 1979

Die nachstehende Arbeit wurde im Rahmen des Vertrages zwischen dem Max-Planck-Institut für Plasmaphysik und der Europäischen Atomgemeinschaft über die Zusammenarbeit auf dem Gebiete der Plasmaphysik durchgeführt.

Electric model of the vacuum vessel of ZEPHYR

Introduction

The magnetic fields necessary for the operation of ZEPHYR will induce large eddy currents on the different tokamak components. These eddy currents will disturb the plasma equilibrium field and will interact mutually and with the external magnetic fields, imposing electromagnetic forces on the different components.

In the case of the vacuum vessel, these electromagnetic forces greatly exceed the atmospheric pressure load, while perturbations of the equilibrium field are mainly caused by the eddy currents flowing on the TF coils. It is therefore necessary to determine precisely the eddy current distributions on the vacuum vessel and the TF coils during the design phase of the experiment because of their decisive influence on the level of mechanical stress on the vacuum vessel and on the vertical stability of the plasma during its adiabatic compression.

Various methods of calculating eddy current distributions have recently been developed, but their accuracy will not be high for such complicated structures as the vacuum vessel or the TF coils of ZEPHYR, because of the limited computer storage capacity or the approximations made.

More exact results can be achieved in a shorter time with an electric model of the tokamak system. By transforming the scales of time and space in an adequate manner just so that the material constants, all currents and all electric and magnetic fields in the tokamak system can be measured on the model. These transformation theorems are derived in the first section, while their applications to the vacuum vessel are described in the second one.

I. Electric similarity theorems

The similarity theorems were derived from Maxwell's equations, which can be written as

$$\mathrm{rot}\,\mathcal{H} = \mu_0 \cdot j + \mu_0 \cdot \mathrm{rot}\,\vec{M} \qquad (1)$$

$$\mathrm{rot}\,\mathcal{E} = -\frac{\partial}{\partial t}\mathcal{B} \qquad (2)$$

$$\mathcal{E} = \varrho \cdot j \qquad (3)$$

$$\mathrm{div}\, j = 0 \qquad (4)$$

j = conduction current,

$j_M = \mathrm{rot}\,\vec{M}$ = magnetization current,

$j_c = \varepsilon_0 \frac{\partial \mathcal{E}}{\partial t} + \frac{\partial P}{\partial t}$ = capacitive current.

The capacitive current will be neglected in eq.(1) for measuring times $\Delta t \ll \frac{1}{c}$,

l = dimension of tokamak system,

c = velocity of light

defining therefore an upper limiting frequency $w_g = \frac{2\pi c}{l}$.

The conduction current can be separated into three parts:

$j = j_L + j_R + j_{C'}$,

inductive $j_L = \mathcal{E}_L/\varrho$ with $\mathrm{rot}\,\mathcal{E}_L \neq 0$

ohmic $j_R = \mathcal{E}_R/\varrho$ with $\mathrm{rot}\,\mathcal{E}_R = 0$

"capacitive" $j_{C'}$, flowing in condcutors,

allowing for $\mathrm{div}\,(j_C + j_{C'}) = 0$ at the interfaces between conductors and media.

Denoting all quantities belonging to a separate tokamak component (vessel, TF coil...) by an index K, the transformations of time, coordinates and resistivities can be written as

model		original		
r_K^+	$= a \cdot r_K$		K=1,2 ...	(5a)
t^+	$= \Omega \cdot t$			(5b)
ϱ_K^+	$= \alpha_K \cdot \varrho_K$			(5c)

The desired transformation of the different current distributions j, j_M and j_C in the components K is given by

$$j_K^+(r,t) = g_K \cdot j_K\left(\frac{r}{a}, \frac{t}{\Omega}\right) \qquad (6).$$

Using this statement for the transformation of current distributions, the transformation of the magnetic field can be derived from Biot-Savart's law

$$\mathcal{B}(r,t) = \frac{\mu_0}{4\pi} \sum_K \int_{V_K} \frac{j_{GK}(r',t) \times (r - r_K')}{|r - r_K'|^3} \, dV_K' = \sum_K \mathcal{B}_K(r,t) \tag{7}$$

$j_{GK} = j_K + j_{MK}$.

By using eqs. (6), (7) and (5) the magnetic field on the electric model $\mathcal{B}^+$ can be calculated:

$$\mathcal{B}^+(r,t) = \frac{\mu_0}{4\pi} \sum_K \int_{V_K^+} \frac{j_{GK}^+(r^{+\prime},t) \times (r - r_K^{+\prime})}{|r - r_K^{+\prime}|^3} \, dV_K^{+\prime} =$$

$$= \frac{\mu_0}{4\pi} \cdot a^3 \sum_K g_K \int_{V_K} \frac{j_K(r_K', \frac{t}{\Omega}) \times (r - a\, r_K')}{|r - a\, r_K'|^3} \, dV_K' \tag{8}.$$

The transformation law of the magnetic field can be derived from eqs. (7) and (8):

$$\mathcal{B}^+(r,t) = a \cdot \sum_K g_K \, \mathcal{B}_K\left(\frac{r}{a}, \frac{t}{\Omega}\right) \tag{9a}.$$

The magnetic flux through a closed loop in the component m of the electric model is given by

$$\Theta_m^+(t) = \int_{F_m^+} \mathcal{B}^+(r^+,t) \, d\vec{F}^+ = a^3 \sum_K g_K \int_{F_m} \mathcal{B}_K(r, \frac{t}{\Omega}) \, d\vec{F} = a^3 \sum_K g_K \Theta_{mK}\left(\frac{t}{\Omega}\right) \tag{9b}.$$

Equation (2), integrated along a closed loop in the component m of the tokamak system, yields

$$\oint_{C_m} \mathcal{E}_L(r,t) \, d\gamma = -\frac{d}{dt} \Theta_m(t)$$

which can be written by means of $\mathcal{E}_L(r,t) = \varrho_m \cdot j_L(r,t)$ as

$$\varrho_m \oint_{C_m} j_L(r,t) \, d\gamma = -\sum_K \int_{F_m} \frac{\partial}{\partial t} \mathcal{B}_K(r,t) \, d\vec{F} \tag{10a}.$$

A similar relation yields for the model

$$\varrho_m^+ \oint_{C_m^+} j_L^+(r^+,t) \, d\gamma^+ = \sum_K \int_{F_m^+} \frac{\partial}{\partial t} \mathcal{B}_K^+(r^+,t) \, d\vec{F}^+ \tag{10b}$$

Inserting eqs. (5), (6) and (9a) in eq. (10b), one gets

$$\alpha_m \cdot \varrho_m \cdot g_m \oint_{C_m} j_L(r, \tfrac{t}{\Omega})\, dr = -a^2 \sum_K g_K \int_{F_m} \frac{\partial}{\partial t} \mathcal{D}_K(r, \tfrac{t}{\Omega})\, d\vec{F} =$$

$$= -a^2 \sum_K g_K \int_{F_m} \frac{1}{\Omega} \frac{\partial}{\partial t} \mathcal{D}_K(r,t)\Big|_{t=\frac{t}{\Omega}} \cdot d\vec{F} \qquad (11)$$

The first similarity theorem can easily be derived from eqs. (10a) and (11) by comparing the coefficients with the same index, yielding

$$\frac{a^2}{\Omega} \cdot \frac{g_K}{g_m} \cdot \frac{1}{\alpha_m} = 1 \qquad \begin{matrix} K = 1,2 \ldots \\ m = 1,2 \ldots \end{matrix}$$

and hence

$$g_K = g \qquad K = 1,2 \ldots$$
$$\alpha_K = \alpha$$

$$\boxed{a^2 = \Omega \cdot \alpha} \qquad (12)$$

Inserting eq. (10b) in eq. (10a) yields the transformation law for the electric field $\mathcal{E}_L$

$$\mathcal{E}^+(r,t) = \frac{a^2 \cdot g}{\Omega} \cdot \mathcal{E}(\tfrac{r}{a}, \tfrac{t}{\Omega}) \qquad (13).$$

The same relation is valid for the field $\mathcal{E}_R$, as can be shown with eqs. (3), (6) and (12):

$$\mathcal{E}^+(r,t) = \varrho^+ \cdot j_R^+(r,t) = \alpha \cdot \varrho \cdot g \cdot j_R(\tfrac{r}{a}, \tfrac{t}{\Omega}) = \frac{a^2 \cdot g}{\Omega} \cdot \mathcal{E}(\tfrac{r}{a}, \tfrac{t}{\Omega})$$

A second similarity theorem can be derived from the transformation law of the capacitive current :

$$j_C^+(r,t) = g \cdot j_C(\tfrac{r}{a}, \tfrac{t}{\Omega})$$

which can be written as for linear media as

$$\varepsilon_0 g \Omega \cdot \mathcal{E}(r, \tfrac{t}{\Omega}) + g \Omega \cdot P(r, \tfrac{t}{\Omega}) = \varepsilon_0 \mathcal{E}^+(ar,t) + P^+(ar,t) \qquad (14).$$

By reason of the continuity of the tangential component of $\underline{\mathcal{E}}$ at the interfaces between conductors and media eq. (13) is valid and can be inserted in eq. (14) with the result

$$\boxed{a^2 = \Omega^2} \tag{15}$$

For linear media, the transformation of the dielectric susceptibility can easily be derived from eqs. (14) and (13)

with $\underline{P}(\underline{r},t) = \varepsilon_0 \overleftrightarrow{\chi}_e(\underline{r}) \cdot \underline{\mathcal{E}}(\underline{r},t)$

and $q \cdot \Omega \overleftrightarrow{\chi}_e(\underline{r}) \underline{\mathcal{E}}(\underline{r},\frac{t}{\Omega}) = \overleftrightarrow{\chi}_e^{+}(a\underline{r}) \underline{\mathcal{E}}^{+}(a\underline{r},t) = \overleftrightarrow{\chi}_e^{+}(a\underline{r}) \cdot \frac{a^2 \cdot q}{\Omega} \underline{\mathcal{E}}(\underline{r},\frac{t}{\Omega})$

$$\overleftrightarrow{\chi}_e(\underline{r}) = \overleftrightarrow{\chi}_e^{+}(a\underline{r}) \qquad \text{or} \qquad \varepsilon_r(\;) = \varepsilon_r^{+}(a\underline{r}) \tag{16}.$$

Similarly, the transformation of the magnetic susceptibility $\overleftrightarrow{\chi}_M$ can be derived from

$$\underline{j}_M^{+}(\underline{r},t) = q \cdot \underline{j}_M(\frac{\underline{r}}{a},\frac{t}{\Omega})$$

With the definition $\underline{M}(\underline{r},t) = \overleftrightarrow{\chi}_M(\underline{r}) \cdot \underline{\mathcal{E}}(\underline{r},t)$ one gets together with eq. (9a)

$$\overleftrightarrow{\chi}_M(\underline{r}) = \overleftrightarrow{\chi}_M^{+}(a\underline{r}) \qquad \text{and} \qquad \mu_r(\underline{r}) = \mu_r^{+}(a\underline{r})$$

Using eqs. (12) and (15), the general similarity theorem can be written as

$$\boxed{a = \Omega = \alpha} \tag{17}.$$

II. Electric model of the ZEPHYR vacuum vessel

The vacuum vessel of ZEPHYR is composed of double-walled thick shell sectors and single or double-walled bellow sections[+)], using Inconel 625 as wall material everywhere.

The easiest way to get reliable results about the behaviour of eddy currents on such an evolved structure will be by measurements in an electric model of the vacuum vessel. During the first design phase, it is sufficient to know the chief eddy current distributions on the vessel during the different time varying phenomena and the influence of the main openings on the eddy currents.

Since the wall thickness of the proposed vessel is much smaller than the radii of curvature at any surface location, the real vacuum vessel can be approximated by single-walled flat shell sections which represent the shell sectors and the bellows sections. Measurements in a corresponding single-walled model of the vacuum vessel will therefore yield sufficiently accurate results as a basis for the design and the stress analysis of the vessel structure. Towards the end of the design phase, when the main vessel geometry is fixed, a more accurate electric model should be built to allow the study of vessel components and openings with diameter smaller than the vessel thickness.

The single-walled vessel approximation is composed of shell sectors with the equivalent thickness $d_s^+ = 2 \cdot d_s$,
d_s = single-shell thickness of the original vessel,
and bellows sections with an equivalent thickness in the toroidal direction d_{bu} and in the poloidal direction d_{bv}

+) Such a vessel concept will be favoured if the tape-wound toroidal-field magnet is used. The decision whether single or double-walled bellow sections will be used depends mainly on the tritium safety restrictions imposed by the Government.

$$d_{bu} = 2 \cdot d_b \cdot \frac{l_{bs}}{l_b} \quad (18), \qquad d_{bv} = 2 \cdot d_b \cdot \frac{l_b}{l_{bs}} \quad (19),$$

d_b = thickness of single real bellows,

l_b = real toroidal length of single bellows,

l_{bs} = toroidal length of bellows sector.

For the model of the vacuum vessel of ZEPHYR, the geometry factor a was chosen as

$$a = 0.2$$

to get a sufficiently high geometric resolution of the current measurements and to limit the mechanical outlay for the model. It can be seen from eq.(17) that for an exact electric model there exists only one transformation factor for space, time or frequency and for every conductor material used.

In most cases, these conditions cannot be fulfilled altogether. For instance, the "toroidal" thickness d_{bu} cannot be diminished by a factor 0.2 in the model because it is not feasible. But simplifications are possible in the case of "thin" shells or "thin" conductors and flanges, i.e. the thickness of the shell of the transverse dimensions of the conductor are small compared with the radii of curvature.

The ratio of resistivity to thickness can be transformed for a "thin" shell by a unique factor $K = \frac{\alpha}{a}$ +):

$$\left(\frac{\varrho}{d}\right)^+ = \frac{\alpha}{a}\left(\frac{\varrho}{d}\right) \quad (20)$$

and for a "thin" conductor by $K' = \frac{\alpha}{a^2}$ +):

$$\left(\frac{\varrho}{\Delta F}\right)^+ = \frac{\alpha}{a^2}\left(\frac{\varrho}{\Delta F}\right) \quad (21)$$

+) Equations (20) and (21) mean the correct transformation of the time constant of each current mode on the vessel, even if the individual resistivities and geometric dimensions are not transformed correctly.

with ΔF = cross-section of this conductor (or flange),

d = thickness of "thin" shell,

ϱ = resistivity,

which offers (over a certain range of operation) one additionally independent variable for the "thin" shell and two independent variables for a "thin" conductor or flange.

It is not necessary to consider eq.(15) for the investigation of magnetic field diffusion through the vessel because of the low upper frequency limits, even for a hard plasma disruption. But it should be kept in mind that by using only eq. (12) the capacitive currents on the original vessel are not transferred accurately to the vessel model. The mismatch between the accurately transferred capacitive current j_c^+ and the capacitive current $j_c^{+'}$ transferred by eq. (12) only is given by

$$j_c^{+'} = \frac{a^2}{\Omega^2}\, j_c^+ \qquad +) \qquad (22)$$

If it is intended to measure the currents or magnetic fields in an electrical model by magnetic probes and Rogowski coils in the frequency domain, it would be desirable to raise the frequencies as high as possible to increase the probe measuring sensitivity. For a given geometry factor a it is possible, by using only eq. (12), to choose a time factor Ω' which is smaller than Ω :

$$\Omega' < \Omega$$

This frequency increase will only be limited by eq. (2), e.g. the capacitive current $j_c^{+'}$ should be much smaller than the measuring error of the vessel currents.

+) Equation (22) is only valid when $(a^2/\Omega^2) = 1 + \varepsilon$ with $|\varepsilon| << 1$, e.g. $j_c' << (j_L + j_R)$.

The poloidal cross-section and a top view of the electric model for the ZEPHYR vacuum vessel with double-walled bellows sections are shown in Fig.1. The model of the bellows sections will consist of 1.5 mm thick stainless steel, simulating the toroidal resistance, while the smaller poloidal resistivity will be simulated by poloidal flanges with correspondingly increased thickness. This approximation of the bellows geometry should yield good accuracy, but a proof of the results by using two accurate models of a bellows section should be done later. The materials and wall thicknesses d of the shell and bellows sections of the model, together with its transformation constants, are listed in Table 1.

Table 1: Data of the electric vessel model with double bellows.

	bellows section	shell sector
a	0.2	0.2
Ω	0.3	0.3
$(\frac{d}{a})$	0.65	0.66
d^+	0.15 cm [1]	0.1 cm
d	0.16 cm [2]	1.6 cm
material$^+$	stainless steel	brass
ϱ^+	$73 \times 10^{-8} \frac{V}{A} \cdot m$	$5 \times 10^{-8} \frac{V}{A} \cdot m$
ϱ	$120 \times 10^{-8} \frac{V}{A} \cdot m$ [3]	$120 \times 10^{-8} \frac{V}{A} \cdot m^2$ [2]
cross-section of flange ΔF^+	1.13 cm^2	0.25 cm^2
alternative flanges	0.4 cm^2	0.30 cm^2

1) $\frac{l_b}{l_{bs}} = 2.5$

3) resistivity of Inconel 625 at LN_2 temperature

2) toroidal thickness of double-bellows section

The value of Ω is relatively large, but it is difficult to lower it further. This would only be possible by raising the factor (α/a) and with it the resistivity of the materials used. The wall thickness cannot be diminished further owing to mechanical stability problems.

III. Method of measuring eddy currents

The eddy current distributions in the shell and bellows surfaces will be determined by measuring the toroidal and poloidal components of the magnetic fields, which are tangential to the model surface at the inside and outside.

The toroidal eddy current j_t^+ can be derived from

$$\vec{j}_t^+ = \vec{n}_1 \times [\mathcal{G}_{p_{t_1}}^+ - \mathcal{G}_{p_{t_2}}^+] = (H_{p_{t_1}}^+ - H_{p_{t_2}}^+) \cdot \vec{n}_t$$

and the poloidal current j_p from

$$\vec{j}_p^+ = \vec{n}_1 \times [\mathcal{G}_{t_1}^+ - \mathcal{G}_{t_2}^+] = (H_{t_2}^+ - H_{t_1}^+) \cdot \vec{n}_p$$

with

$$\mathcal{G}_{p_t}^+ = H_{p_t}^+ \cdot \vec{n}_p \quad \text{and} \quad \mathcal{G}_t^+ = H_t^+ \cdot \vec{n}_t$$

where the index 1 denotes the region outside the vessel model and the index 2 the inner region of it (see Fig.2).

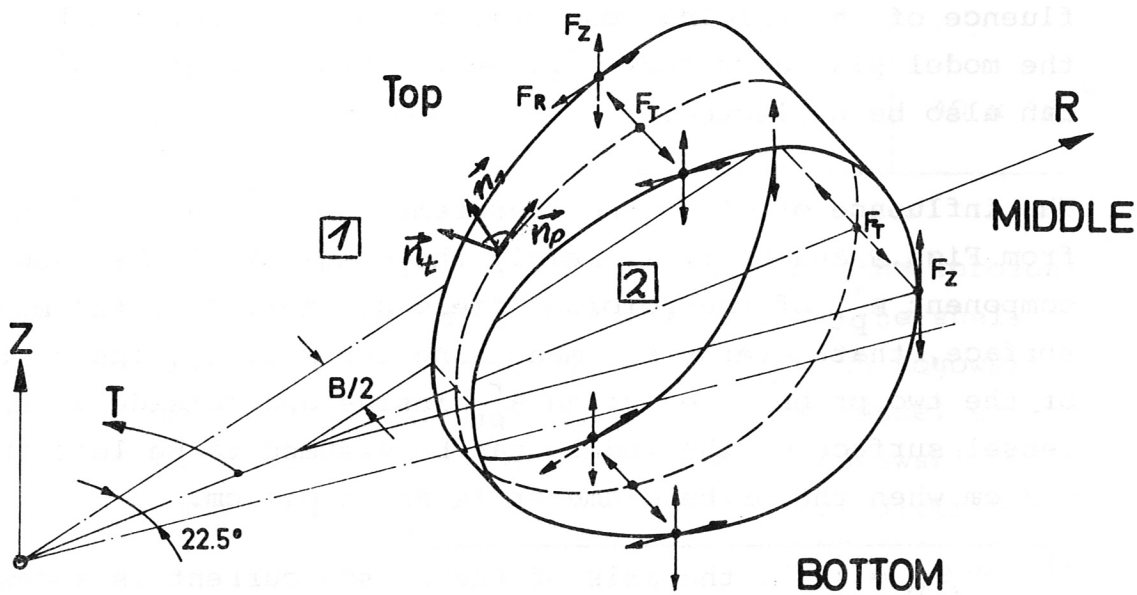

Fig. 2

The main reason for building an electric model of the vacuum vessel will be to evaluate the eddy currents on the vessel, induced by disruption of the plasma current. To simulate the plasma current a current will be passed through a thin conductor along the centre line of the model plasma [+)]. It is intended to measure in the frequency domain and calculate the real-time behaviour with the corresponding Fourier integrals.

At any surface point of the model, the magnetic fields $\mathcal{G}^{+}_{t1,2}$ and $\mathcal{G}^{+}_{Pt1,2}$ will be measured simultaneously by four magnetic probes forming a rectangle. One pair records the magnetic field at the inside and one pair that outside the vessel surface.

The axis of the magnetic probes must always be adjusted parallel to the surface of the model, in the directions of $\vec{n}_t$ and $\vec{n}_p$. Since the eddy current components j^{+}_t and j^{+}_p will be measured directly by a difference method, the influence of the normal component of the magnetic field on these measurements can then be neglected. By correct adjustment of the probes in the directions of $\vec{n}_t$ and $\vec{n}_p$, the influence of the poloidal magnetic field B^{+}_p, generated by the model plasma current I^{+}_{pl}, on the measurement of j^{+}_p can also be neglected.

The influence of B^{+}_p on the measurement of j^{+}_t can be deduced from Figs. 3 and 4. It is mainly the gradient of the tangential component B^{+}_{pt} of the poloidal field B^{+}_p, normal to the model surface, that governs the measuring error of j^{+}_t. The distance of the two probes, measuring B^{+}_{pt} inside and outside at the vessel surface of the model, can be assumed to be less than 0.3 cm when the probe diameter is about 0.1 cm.

[+)] For β_p = 1.35, the axis of the plasma current is somewhat shifted outwards from the plasma centre line towards larger major radii. The variation of the electromagnetic force and eddy currents with the position of the plasma current axis will be studied separately.

Figure 5 shows the measuring error of j_t^+, with reference to a maximum mean toroidal current $\langle j_t^+ \rangle = I_{pl}^+ / l_p^+$ in the wall of the vessel model and to a distance of 0.3 cm between the two B_{pt}^+ probes. It can be seen from Fig.5 that high-accuracy measurements of j_t^+ at the throat of the vessel model can only be achieved by subtracting the difference probe signals for I_{pl}^+ without the vessel from the signals with the vessel model. A second method of increasing the accuracy will be the use of phase sensitive amplifiers, while the recording and handling of data will be achieved with multi-channel transient digitizers coupled directly to a PDP 11 computer. The frequency range and the expected signal levels are represented in Table 2.

Table 2:

	probe difference signal (μV)	current density $\langle j^+ \rangle$ in the wall (A/m)	equivalent probe surface (m^2)
Upper frequency limit $\nu_{gu} = 3 \times 10^5\ s^{-1}$	95	1	40×10^{-6}
Lower frequency limit $\nu_{gl} = 1.6 \times 10^2\ s^{-1}$	0.05	1	40×10^{-6}

The eddy currents along the poloidal flanges and the toroidal currents through the vertical symmetry planes of the shell and bellows sectors will be measured directly with Rogowski coils. Two small toroidal slits (1x5 mm) in the vessel surface (see Fig.1) allow the fixing of a slotted Rogowski belt, causing only minor distortion of the eddy current distribution.

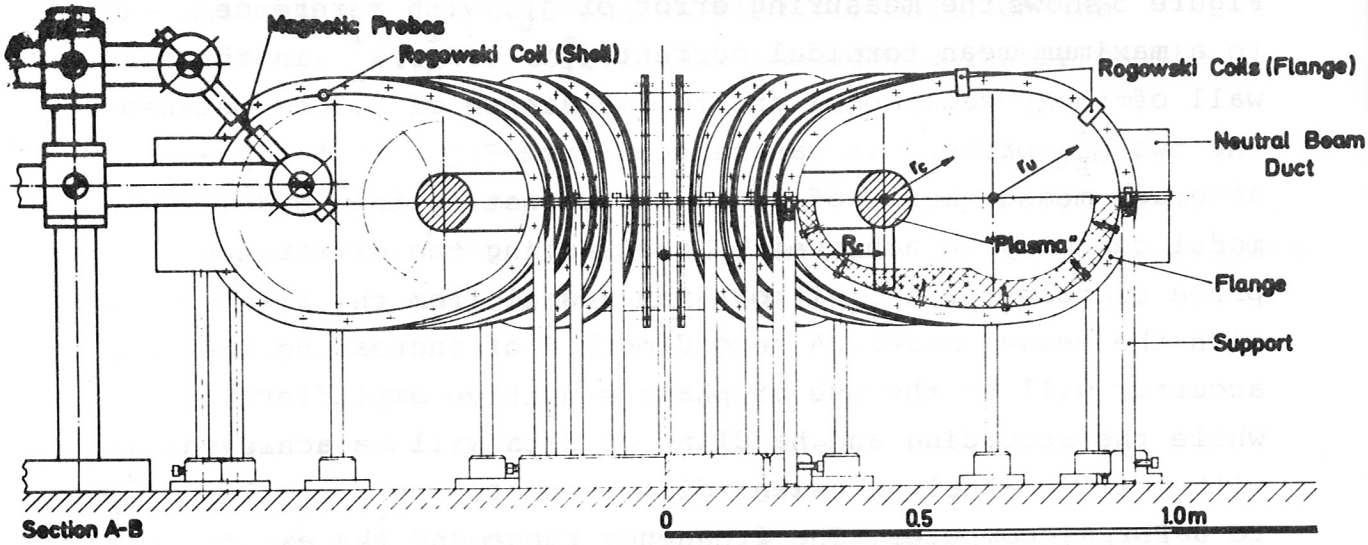
Magnetic Probes
Rogowski Coil (Shell)
Rogowski Coils (Flange)
Neutral Beam Duct
rc
ru
Rc
"Plasma"
Flange
Support
Section A-B
0
0.5
1.0m

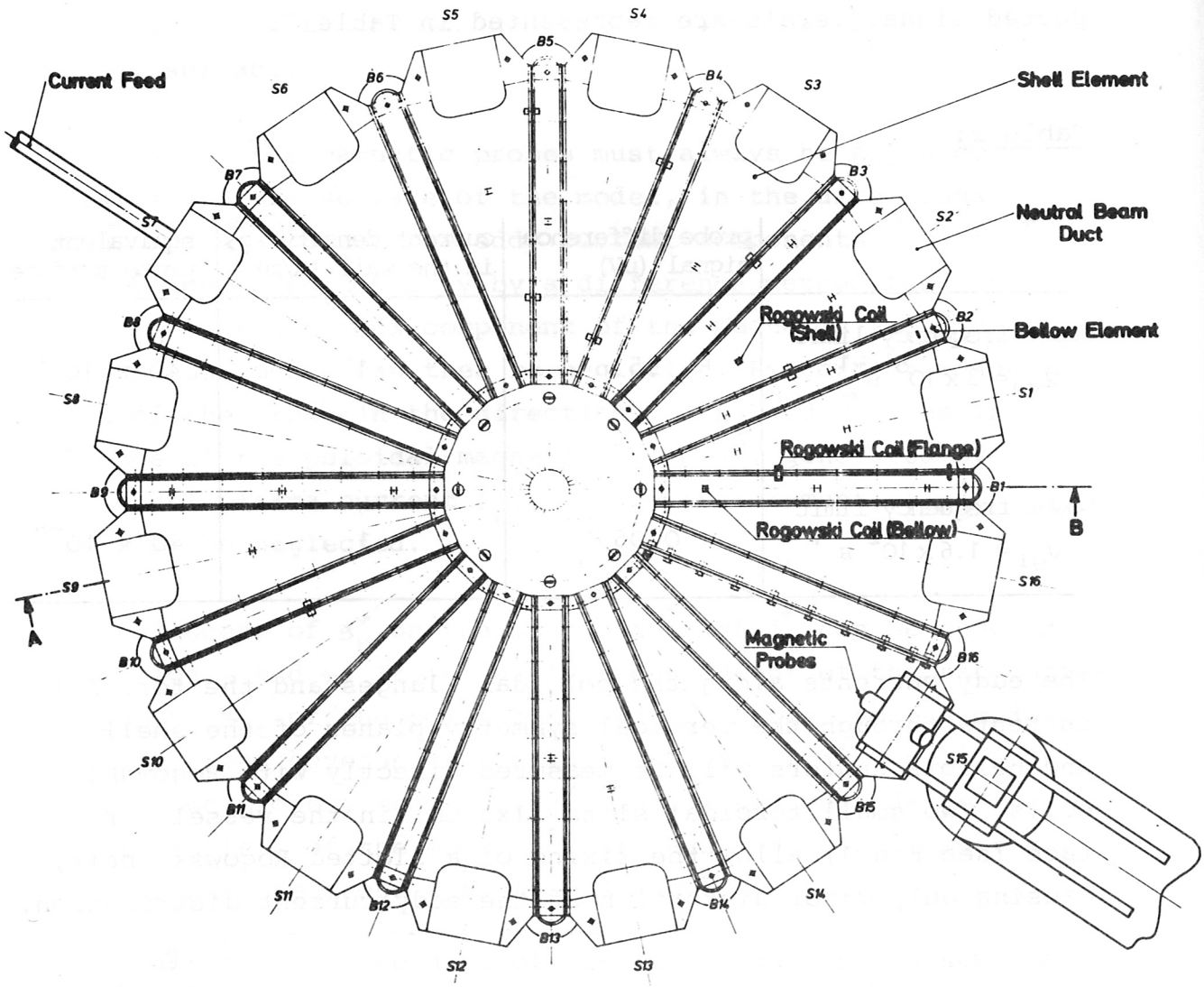
Current Feed
Shell Element
Neutral Beam Duct
Rogowski Coil (Shell)
Bellow Element
Rogowski Coil (Flange)
Rogowski Coil (Bellow)
Magnetic Probes
A
B
S1
S2
S3
S4
S5
S6
S7
S8
S9
S10
S11
S12
S13
S14
S15
S16
B1
B2
B3
B4
B5
B6
B7
B8
B9
B10
B11
B12
B13
B14
B15
B16

Fig. 1

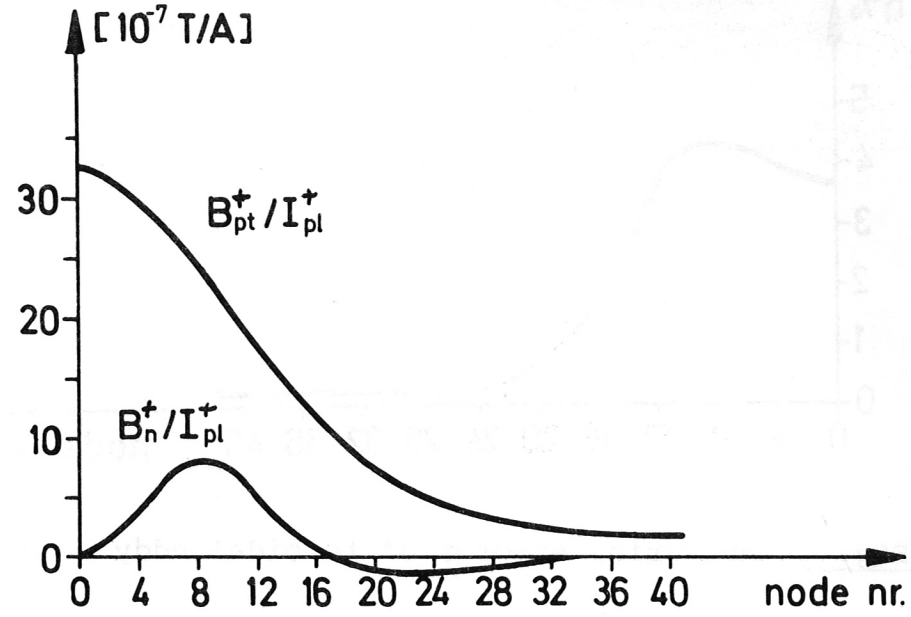
[10⁻⁷ T/A]
30
20
10
0
B^+_{pt}/I^+_{pl}
B^+_n/I^+_{pl}
0 4 8 12 16 20 24 28 32 36 40
node nr.

Fig. 3

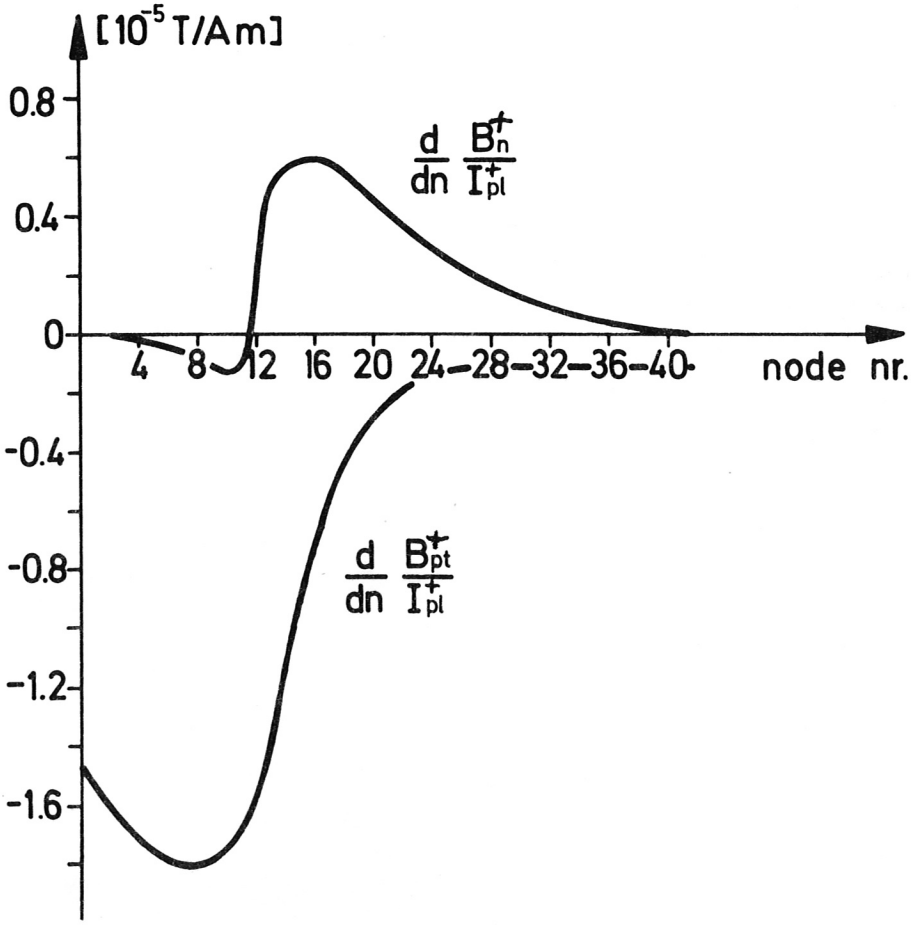
[10⁻⁵ T/Am]
0.8
0.4
0
-0.4
-0.8
-1.2
-1.6
$\frac{d}{dn}\frac{B^+_n}{I^+_{pl}}$
$\frac{d}{dn}\frac{B^+_{pt}}{I^+_{pl}}$
4 8 12 16 20 24 28 32 36 40
node nr.

Fig. 4

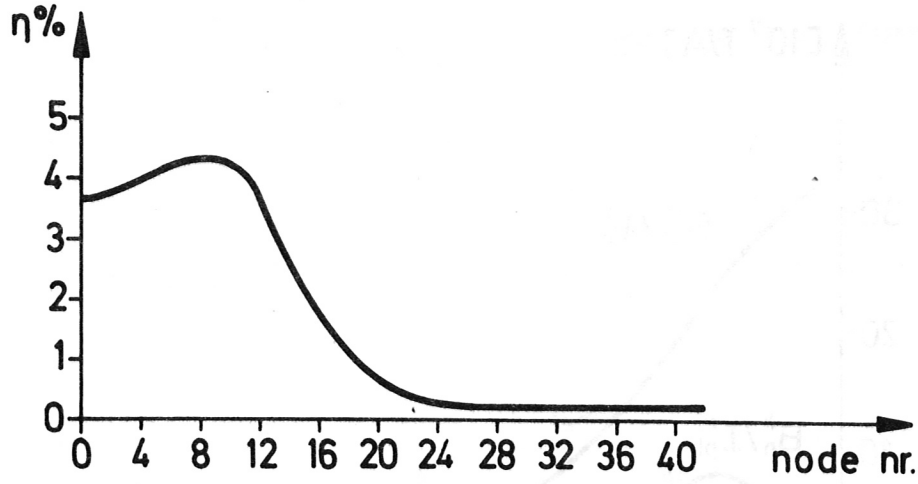

Fig. 5 Measuring error η of toroidal eddy currents